Nanometer-Range Strain Distribution in Layered Incommensurate Systems

Oleksandr Stetsovych,[1] Filip Dvořák,[1] Lucie Szabová,[1] Stefano Fabris,[2,3] Josef Mysliveček,[1,*] and Vladimír Matolín[1]

[1]*Charles University, Faculty of Mathematics and Physics, V Holešovičkách 2, Praha 8, Czech Republic*
[2]*CNR-IOM DEMOCRITOS, Theory@Elettra Group, Istituto Officina dei Materiali, Strada Statale 14 km 163,5 in AREA Science Park, I-34149 Trieste, Italy*
[3]*SISSA, Scuola Internazionale Superiore di Studi Avanzati, via Bonomea 265, I-34136 Trieste, Italy*

(Received 28 August 2012; published 26 December 2012)

We adopt fringe counting from classical moiré interferometry on moiré patterns observed in scanning tunneling microscopy of strained thin films on single crystalline substrates. We analyze inhomogeneous strain distribution in islands of $CeO_2(111)$ on Cu(111) and identify a generic source of strain in heteroepitaxy—a thickness-dependent lattice constant of the growing film. This observation is mediated by the ability of ceria to glide on the Cu substrate. The moiré technique we are describing has a potential of nanometer-scale resolution of *inhomogeneous* two dimensional strain in incommensurate layered systems, notably in supported graphene.

DOI: 10.1103/PhysRevLett.109.266102 PACS numbers: 68.35.Gy, 68.37.Ef, 68.55.−a, 81.15.Aa

Mapping of strain distribution in nanometer-sized objects represents a challenge of current experimental nanoscience. Strain crucially influences transport properties of electronic devices [1,2], chemical reactivity of nanostructured catalysts [3–5], and growth mode and stability of thin film [6] and nanostructured systems [7]. In extreme cases strain in nanostructures can be viewed in a microscope as the real-space distortion of the atomic lattice [5], however, indirect microscopic methods prevail.

Many indirect microscopic observations take advantage of the so-called moiré—beats between two periodic lattices. For nanometer scale resolution, one lattice is always the atomic lattice of the subject, the other is a known reference in the form of a bulk single crystal (transmission electron microscopy) [8,9], scanning raster of the image frame (scanning transmission electron microscopy, scanning probe microscopy) [10,11], or, in the case of layered systems, single crystal substrate or adlayer (scanning probe microscopy) [12,13]. Tiny variations in the registry of the lattices become greatly amplified by the moiré effect. Thus, using moiré, small changes in the lattice constant [14] or in the azimuthal registry of the lattices can be measured with unprecedented precision [15]. In systems with moiré also imperfections of the atomic lattices stand out very clearly facilitating visualisation and study of dislocations and domain boundaries [10,12,16].

Majority of existing quantitative studies analyze homogeneous moiré and yield space-averaged information on lattice constants and/or azimuthal rotation [14,17,18]. Only recently, moiré-based mapping of inhomogeneous strain became available in transmission electron microscopy [9]. In layered systems observed with scanning probe methods, the potential of moiré for strain analysis has long been realized [13], however, two-dimensional analysis of inhomogeneous strain has been missing so far.

Here we present a study of inhomogeneous honeycomb moiré observed by scanning tunneling microscope (STM) in oxide-on-metal system $CeO_2(111)/Cu(111)$. Ceria is a featured material for heterogeneous catalysis [19,20] and a prospective high-k dielectric [21]. From the inhomogeneities of the moiré we reconstruct distribution of local strain in ceria islands. We consider the moiré as a superposition of interference fringes and adopt a well-established method of fringe counting [22]. We observe that ceria layers can freely adapt their lateral extension by gliding on the Cu (111) substrate and undergo elastic in-plane deformation dictated by boundary conditions and defects of a particular ceria flake. For freestanding defect-free multilayer ceria islands finite element calculations show that the strain distribution corresponds to equilibrium of mutually confined (concentric) areas with thickness-dependent lattice constants and free outer boundary. The described method for analysis of strain distribution in incommensurate layered systems is expected to be generally applicable, particularly in supported graphene [23].

Ceria islands on Cu(111) were prepared and observed in an ultra-high-vacuum chamber with base pressure 1×10^{-8} Pa with standard sample cleaning and preparation facilities and a homemade STM. Ce was evaporated on clean Cu(111) substrate kept at 400 °C in a background atmosphere of 5×10^{-5} Pa O_2 to a total amount of 0.5 monolayer (ML) CeO_2. 1 ML CeO_2 is a vertical stack of O—Ce—O with 7.9×10^{14} cm^{-2} Ce atoms. A detailed account of the sample preparation and the morphology of the obtained samples has been published recently [24]. We obtain flat $CeO_2(111)$ islands 1–3 ML thick residing on clean Cu(111). In between the islands, Cu is oxidized. $CeO_2(111)$ is incommensurate on Cu(111). About 45% of the islands in the population show a honeycomb moiré in the first few monolayers (ML). In these islands, $[\bar{1}\,\bar{1}\,2]$ directions of ceria and Cu are antiparallel [24]. Remaining islands show different azimuthal orientations and different coincidence structures and will not be discussed here.

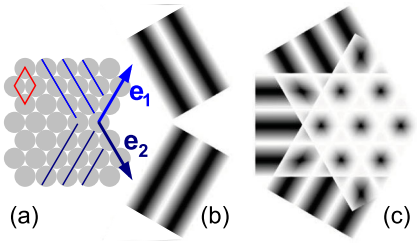

FIG. 1 (color online). Moiré as superposition of interference fringes. (a) (111) substrate. Rhombus: substrate unit cell; lines: substrate atoms as reference grating; $\mathbf{e}_1$, $\mathbf{e}_2$: two independent directions. (b) Orientation of interference fringes corresponding to strain in the (111) overlayer in $\mathbf{e}_1$ and $\mathbf{e}_2$ directions. (c) Moiré in the overlayer formed by two independent and one dependent set of fringes.

In engineering [22], strain is determined from a projection of a linear reference grating on a strained sample grating. This projection yields fringes—stripes in the sample plane that can be numbered consecutively. The displacement in the sample plane normal to the reference grating is $U(x, y) = a_0 N(x, y)$, where a_0 is a pitch of the reference grating, N is a number of a fringe (fringe order), and x, y in-plane coordinates of a fringe. $U(x, y)$ is scalar; vector displacement is obtained repeating the procedure with the reference grating rotated by 90°.

The honeycomb moiré of two (111) atomic lattices can be considered as a superposition of fringes from two linear reference gratings intersecting at an angle of 60°, see the schematic in Fig. 1. The lines of the reference gratings coincide with close-packed rows of the single crystal substrate with directions $\mathbf{e}_1$, $\mathbf{e}_2$ [Fig. 1(a)]. Uniaxial strain in the sample along $\mathbf{e}_1$ yields fringes parallel to $\mathbf{e}_2$ and vice versa [Fig. 1(b)]. Typically, the strain in the sample is close to homogeneous; in this case, fringes parallel to $\mathbf{e}_1 - \mathbf{e}_2$ complete the honeycomb moiré appearance [Fig. 1(c)]. The vector displacement in the sample plane is $\mathbf{U}(x, y) = a_0 N_1(x, y)\mathbf{e}_1 + a_0 N_2(x, y)\mathbf{e}_2$, where a_0 is a size of the surface unit cell of the reference single crystal, and $N_1(x, y)$ and $N_2(x, y)$ are fringe orders corresponding to $\mathbf{e}_1$ and $\mathbf{e}_2$. Zero displacement corresponds to samples that are pseudomorphic with the substrate.

A reconstruction of two-dimensional strain distribution is illustrated in Fig. 2. Figure 2(a) shows the STM topograph of a 1 ML thick ceria island in a complex boundary condition. Top left is a Cu step edge covered with ceria (white), bottom right 1 ML ceria with different azimuthal orientation (gray), right oxidized copper (black). Boundaries of the ceria domains are partly decorated with 2 ML ceria and/or voids with oxidized copper. A 1 ML ceria shows inhomogeneous moiré. Centers of moiré spots are marked by dots. After selecting $\mathbf{e}_1$, $\mathbf{e}_2$ the moiré spots are assigned integer fringe orders. After numerical interpolation fringes in two directions can be plotted as equipotentials of $N_{1,2}(x, y)$, see Fig. 2(b). $N_{1,2}(x, y)$ converts to vector displacement $\mathbf{U}(x, y)$ that determines the strain.

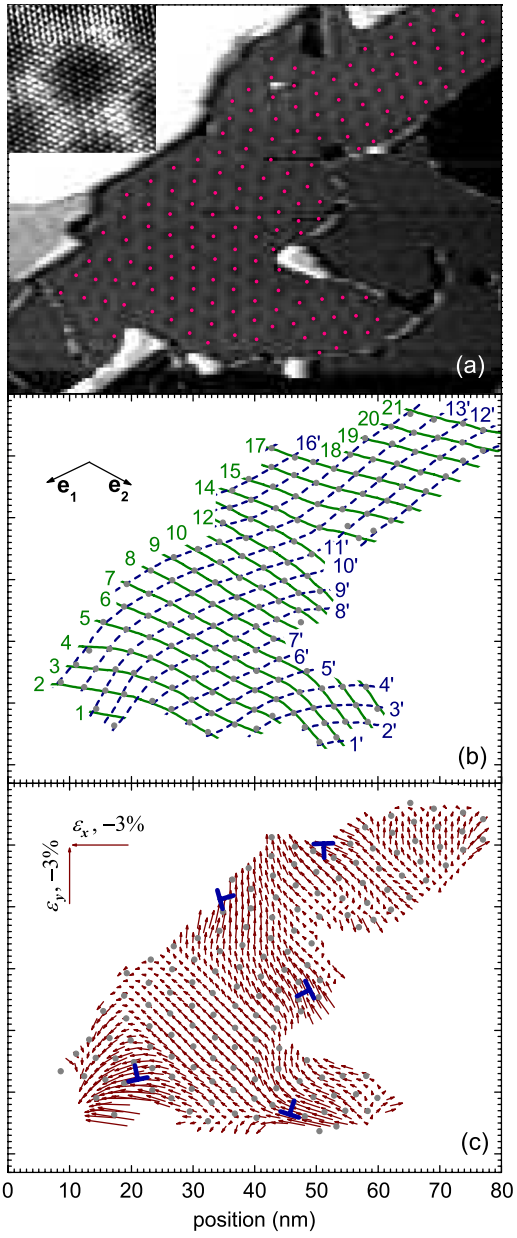

FIG. 2 (color online). (a) Inhomogeneously strained 1 ML ceria/Cu(111). Moiré centers are marked by dots. Inset: atomic resolution of moiré. (b) Moiré fringes and fringe orders corresponding to $\mathbf{e}_1$ (full lines), $\mathbf{e}_2$ (dashed lines). (c) Two-dimensional strain. ε_x and ε_y are plotted as components of 2D arrows. To enhance the local variations, only deviations from a homogeneous 3% contraction (cf. scale in top left corner) are shown. Strain is evaluated relative to bulk ceria. T represent defects in ceria layer. Image width in (a) 80 nm, inset 8 × 8 nm^2.

Strain components $\varepsilon_x = \partial U_x/\partial x$, and $\varepsilon_y = \partial U_y/\partial y$, are plotted in Fig. 2(c).

On average, $\varepsilon_x = \varepsilon_y = -3.2\%$. This corresponds to a homogeneous contraction of ceria monolayer with respect to a commensurate growth of 2 unit cells of $CeO_2(111)$ on 3 unit cells of Cu(111) expected from bulk lattice constants of ceria and copper [24,25]. In addition, local variations of

strain are observed that can be assigned to defects in the ceria monolayer. Typically, a crystallographic defect is accompanied by the appearance or disappearance of a moiré fringe [10,12,16,26]. This is not observed inside the island in Fig. 2(a). Rather, we can estimate locations of (virtual) edge dislocations near the perimeter of the island that contribute to the observed strain distribution. These defects are marked T in Fig. 2(c). The displacement corresponding to these defects is smaller than expected for a developed partial dislocation in ceria ML [26]. Thus, the physical nature of these defects is most likely point defects and pinning of the CeO_2 structure at domain boundaries of the ceria monolayer.

The absence of crystallographic defects inside the island together with the inhomogeneity of the observed moiré allow us to conclude that the ceria monolayer has an ability to respond to external stress by elastic in-plane deformation freely gliding on the copper substrate. Gliding in response to stress is a general property of weakly interacting substrate-adsorbate systems [6]. Recently it has been confirmed, e.g., in an incommensurate system graphene/Ir(111) [14]. In the following, we show that gliding is possible also for thicker ceria. This is in line with theoretical predictions of comparatively small variations (≤ 0.24 eV) of the binding energy of CeO_2(111) on Cu(111) for different mutual lateral shifts [27].

STM topograph of a multilayer ceria island with a free outer boundary on most of its perimeter is shown in Fig. 3(a). The island has a triangular shape in first and higher ceria monolayers indicating a coherent single crystal [24]. This type of island dominates the island population on the prepared samples. First and second ML of the island shows a honeycomb moiré with three characteristic modifications: on the apexes of the 1st ML area, the moiré is isotropic with periodicity corresponding to 3.2% contraction of ceria layer. In the center of the 2nd ML area, the moiré is isotropic with an increased period corresponding to a reduced 2.4% contraction of ceria layer. On the sides of the 1st ML area, the moiré is anisotropic with a periodicity elongated in the direction of the island edge. Strain distribution in the island can be estimated from the shape of selected moiré fringes [dash dotted lines in Fig. 3(a)]. Qualitatively, the increased lattice constant of the 2 ML area causes its lateral expansion and a corresponding outward relaxation of the 1 ML area.

The observed relaxation of the ceria island is mediated by gliding of the layer on the substrate. With gliding, areas where second ceria ML nucleates on top of first ceria ML (or 3rd on 2nd, etc.) can adjust their lateral lattice constant unrestricted by the registry with the substrate. The driving force for changing the lateral lattice constant of the layer is a quantum-mechanical size effect related to a limited thickness of the layer as predicted by *ab initio* calculations [24,28]. The extent of this size effect for ceria can be seen in Table I for the first 3 ML where reference from moiré

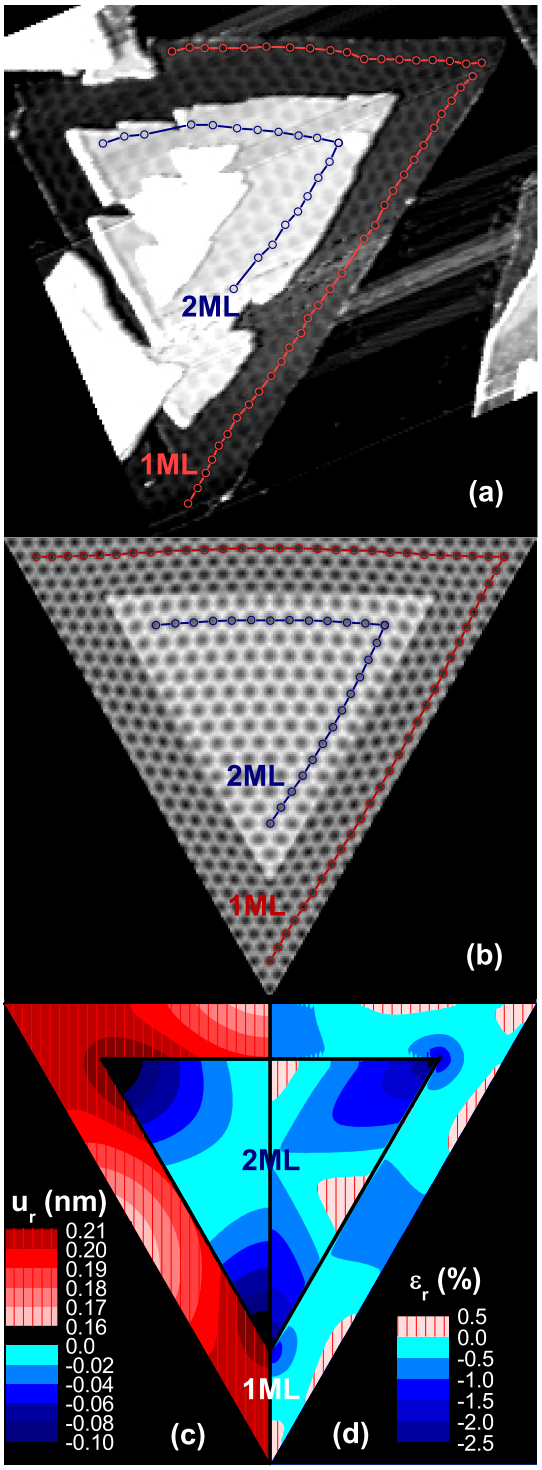

FIG. 3 (color online). (a) Inhomogeneously strained multilayer island of ceria on Cu(111). 1 ML and 2 ML label the first and second monolayers. Rings are moiré centers of a selected constant fringe order, lines are guides to the eye. (b)–(d) Simulation of a strained 2 ML island. 2 ML area features, intrinsically, a larger lattice constant than 1 ML area (cf. Table I). (b) Moiré, (c) radial displacement, (d) radial strain. Displacement and strain are evaluated relative to lattice constants of the homogeneous 1 ML or 2 ML, respectively. Image width in (a), (b) 130 nm, in (c), (d) 65 nm.

TABLE I. Lateral contraction of ceria layers of different thickness with respect to bulk lattice constant. STM: from moiré patterns in discontinuous layers grown on Cu(111) at 400 °C, DFT: from unsupported stoichiometric ceria layers.

Ceria thickness	Contraction (%) STM	DFT
1 ML	3.2 ± 0.3[a]	6.7[a]
2 ML	2.4 ± 0.3[a]	3.7[a]
3 ML	1.9 ± 0.4[b]	2.8[b]

[a]Reference [24].
[b]This work. For technical details of DFT see Ref. [24].

STM data and results of model density functional theory (DFT) calculations are available. DFT refers to unsupported stoichiometric ceria layers. The measured size effect is smaller than the calculated one due to the interaction with the substrate that effectively counteracts the size effect [24,28].

With the assumption of gliding, the strain distribution in the observed island can be modeled as a 2D elastic problem with the role of the substrate reduced to keeping all relaxations in plane. Results of the model obtained with finite element calculation are shown in Figs. 3(b)–3(d). We use a simplified geometry of the island composed only of 1 and 2 ML areas that are equilateral and concentric. Sides of 1 and 2 ML areas are 130 and 80 nm, respectively. The stress in the system originates from a larger lateral lattice constant and a larger stiffness of the inner 2 ML area compared to the outer 1 ML area. Lattice constants reflect the difference between 2.4% and 3.2% contraction with respect to ceria bulk for 2 and 1 ML, the stiffness ratio is taken 3:2 for 2 ML with respect to 1 ML, Poisson's ratio is $1/3$ for both 1 and 2 ML. Relaxation is allowed in a lateral direction with a free outer boundary and a weld between 1 and 2 ML areas.

A simulation of moiré in the relaxed island is shown in Fig. 3(b). The color on the gray scale is proportional to the lateral distance between atoms of ceria layer and Cu substrate. The simulated moiré fully replicates the moiré distribution observed in experiment, as best viewed on the anisotropic moiré along island edge and the shape of the selected fringes. Actually, the shape of any fringe is reproduced with a considerable agreement including fringes that cross the boundary between 1 and 2 ML. Small discrepancies between simulation and experiment can be traced back to the differences between geometry of the real and the idealized island.

Moiré reflects displacements in the relaxed island. The radial component of the displacement is shown in Fig. 3(c). Compared to the unrelaxed state, the 1 ML area moves outward, while the 2 ML area moves inward. The movements are up to 2 Å on the 130 nm island. The radial component of the strain $\varepsilon_r = \partial U_r/\partial r$ is shown in Fig. 3(d). The mutual confinement of the 1 and 2 ML areas causes an extra uniaxial strain in both 1 and 2 ML areas decreasing ε_r by about 1% in the radial direction.

The agreement between the experimental and calculated moiré allows us to define a new generic source of strain in heteroepitaxy—a thickness-dependent lattice constant of the growing film. This finite-size effect will mostly influence strain evolution in weakly interacting incommensurate systems. In the presence of gliding between the substrate and the growing layer, the growing layer is allowed to adopt the lateral lattice constant corresponding to its local thickness. This relaxation is counteracted by elastic interaction between neighboring areas with different thickness leading to strongly inhomogeneous strain distributions. Further, the relaxation can be influenced by crystallographic defects in the growing layer.

On the other hand, finite-size effects on strain will be less pronounced in the well-studied case of heteroepitaxial systems where the growing layer is pseudomorphic [29–32] or commensurate with the substrate [16,33]. In these systems, the lattice constant of the growing layer is initially fixed by the interaction with the substrate overriding the thickness dependence. Indeed, eventual moiré in these systems does not indicate changes of the lattice constant with increasing layer thickness [16,30]. Upon reaching a critical thickness the accumulated stress in these layers relaxes by a variety of coexisting pathways including nucleation of 3D islands [16,29], roughening [29,33], and nucleation of dislocations in the layer [29–31].

To conclude, we have determined and characterized an inhomogeneous strain distribution in ceria islands growing on Cu(111) using an analogy between the moiré interferometry in engineering and moiré observed by scanning tunneling microscope in incommensurate layered systems. Ceria islands growing in height relax the stress in the ceria layer by lateral expansion freely gliding on the Cu substrate. This allows us to identify a new and generic source of strain in heteroepitaxy—a thickness-dependent lattice constant which is a finite-size effect on ultrathin layers several ML thick. The described method of mapping of inhomogeneous strain distribution can be applied generally to incommensurate systems including supported graphene.

This work was supported by the Ministry of Education of the Czech Republic (LH11017, ME08056) and by the Grant Agency of the Czech Republic (GACR 204/11/1183, GACR 202/09/H041). L. S, O. S., and F. D. acknowledge the support from the Grant Agency of the Charles University (GAUK 103410, GAUK 339311, GAUK 610112). International cooperation was supported by COST action CM1104. We would like to thank Dan Mazur for a helpful discussion.

*josef.myslivecek@mff.cuni.cz

[1] F. Schäffler, Semicond. Sci. Technol. **12**, 1515 (1997).
[2] D. A. Antoniadis, I. Aberg, C. Ni Chleirigh, O. M. Nayfeh, A. Khakifirooz, and J. L. Hoyt, IBM J. Res. Dev. **50**, 363 (2006).

[3] M. Mavrikakis, B. Hammer, and J. K. Nørskov, Phys. Rev. Lett. **81**, 2819 (1998).
[4] J. Wintterlin, T. Zambelli, J. Trost, J. J. Greeley, and M. Mavrikakis, Angew. Chem., Int. Ed. **42**, 2850 (2003).
[5] M. J. Walsh, K. Yoshida, A. Kuwabara, M. L. Pay, P. L. Gai, and E. D. Boyes, Nano Lett. **12**, 2027 (2012).
[6] M. Henzler, Surf. Sci. **357–358**, 809 (1996).
[7] V. Holý, G. Springholz, M. Pinczolits, and G. Bauer, Phys. Rev. Lett. **83**, 356 (1999).
[8] G. A. D. Briggs, D. P. Basile, G. Medeiros-Riberio, T. T. Kamins, D. A. A. Ohlberg, and R. Stanley Williams, Surf. Sci. **457**, 147 (2000).
[9] M. Hÿtch, F. Houdellier, F. Hüe, and E. Snoeck, Nature (London) **453**, 1086 (2008).
[10] D. Su and Y. Zhu, Ultramicroscopy **110**, 229 (2010).
[11] H. Shang, H. Xie, Q.-K. Xue, J. Jia, and F. Dai, Scanning **26**, 282 (2004).
[12] O. Rodríguez de la Fuente, M. A. González, and J. M. Rojo, Phys. Rev. B **63**, 085420 (2001).
[13] Y. Gai, Y. He, X. Li, J. F. Jia, and W. S. Yang, Surf. Sci. **365**, 96 (1996).
[14] H. Hattab, H. A. T. N'Diaye, D. Wall, C. Klein, G. Jnawali, J. Coraux, C. Busse, R. van Gastel, B. Poelsema, T. Michely, F.-J. Meyer zu Heringdorf, and M. Horn-von Hoegen, Nano Lett. **12**, 678 (2012).
[15] F. Sedona, S. Agnoli, and G. Granozzi, J. Phys. Chem. B **110**, 15 359 (2006).
[16] M. Ritter, W. Ranke, and W. Weiss, Phys. Rev. B **57**, 7240 (1998).
[17] P. Merino, M. Švec, A. L. Pinardi, G. Otero, and J. A. Martín-Gago, ACS Nano **5**, 5627 (2011).
[18] D. L. Miller, K. D. Kubista, G. M. Rutter, M. Ruan, W. A. de Heer, P. N. First, and J. A. Stroscio, Phys. Rev. B **81**, 125427 (2010).
[19] G. N. Vayssilov, Y. Lykhach, A. Migani, T. Staudt, G. P. Petrova, N. Tsud, T. Skála, A. Bruix, F. Illas, K. C. Prince, V. Matolín, K. M. Neyman, and J. Libuda, Nat. Mater. **10**, 310 (2011).
[20] A. Hornés, A. B. Hungría, P. Bera, A. López Cámara, M. Fernández-García, A. Martínez-Arias, L. Barrio, M. Estrella, G. Zhou, J. J. Fonseca, J. C. Hanson, and J. A. Rodriguez, J. Am. Chem. Soc. **132**, 34 (2010).
[21] J. I. Flege, B. Kaemena, S. Gevers, F. Bertram, T. Wilkens, D. Bruns, J. Bätjer, T. Schmidt, J. Wollschläger, and J. Falta, Phys. Rev. B **84**, 235418 (2011).
[22] D. Post and M. Han, in *Springer Handbook of Experimental Solid Mechanics*, edited by W. N. Sharpe, Jr. (Springer, Berlin, 2008), pp. 627–654.
[23] S. Marchini, S. Günther, and J. Wintterlin, Phys. Rev. B **76**, 075429 (2007).
[24] L. Szabová, O. Stetsovych, F. Dvořák, M. Farnesi Camellone, S. Fabris, J. Mysliveček, and V. Matolín, J. Phys. Chem. C **116**, 6677 (2012).
[25] 2:3 commensurate growth represents zero strain in the present calculation. Since the moiré contrast dominates the STM contrast from 2:3 epitaxy [24], on-top and bridge sites of the substrate are considered equivalent yielding $a_0 = 1/2 a_{\mathrm{Cu}(111)}$ for the evaluation of $\mathbf{U}(x, y)$.
[26] A new fringe requires a displacement of $1/2 a_{\mathrm{Cu}(111)}$ or $1/3 a_{\mathrm{CeO_2}(111)}$ corresponding to, e.g., a partial dislocation in the $CeO_2(111)$ monolayer due to a missing O row.
[27] L. Szabová, M. Farnesi Camellone, M. Huang, V. Matolín, and S. Fabris, J. Chem. Phys. **133**, 234705 (2010).
[28] G. Barcaro, I. O. Thomas, and A. Fortunelli, J. Chem. Phys. **132**, 124703 (2010).
[29] G. Wedler, C. M. Schneider, A. Trampert, and R. Koch, Phys. Rev. Lett. **93**, 236101 (2004).
[30] J. Schoiswohl, W. Zheng, S. Surnev, M. G. Ramsey, G. Granozzi, S. Agnoli, and F. P. Netzer, Surf. Sci. **600**, 1099 (2006).
[31] S. Benedetti, P. Torelli, S. Valeri, H. M. Benia, N. Nilius, and G. Renaud, Phys. Rev. B **78**, 195411 (2008).
[32] D. F. Forster, J. Klinkhammer, C. Busse, S. G. Altendorf, T. Michely, Z. Hu, Y.-Y. Chin, L. H. Tjeng, J. Coraux, and D. Bourgault, Phys. Rev. B **83**, 045424 (2011).
[33] C. Tusche, H. L. Meyerheim, and J. Kirschner, Phys. Rev. Lett. **99**, 026102 (2007).